

Cyclic cone penetrometer tests: worthwhile?

Conleth O'Loughlin^{1#}, Fraser Bransby¹, Senthin Mani², Britta Bienen¹ and Pourya Esfeh¹

¹ Centre for Offshore Foundation Systems, Oceans Graduate School, The University of Western Australia

² Fugro, Perth, Western Australia

[#]Corresponding author: conleth.oloughlin@uwa.edu.au

ABSTRACT

This paper explores the merit of including cyclic episodes in cone penetrometer tests to measure changes in sleeve resistance during cycling. Tests were carried out in a geotechnical centrifuge in a kaolin clay and a dense silica sand. The data from the tests in clay indicate that the cone sleeve mobilises the remoulded undrained shear strength during the initial penetration, but that with continued cycling, the mobilised interface shear strength reduces to around one-third of the remoulded undrained shear strength before increasing. The initial reduction is considered to be due to local consolidation around the cone sleeve (leading to total stress reduction), whereas the subsequent increase is attributed to consolidation-induced strength hardening. Tests in sand also indicate a reduction in sleeve friction during cycling, consistent with the shear band contraction mechanism associated with friction fatigue of piles in sand, but with no consolidation-induced hardening behaviour as these tests were drained. The findings suggest that cyclic cone penetrometer tests may be a convenient means of gathering data for geotechnical design for problems where the cyclic response at the clay/structure interface is of interest. Considerations on the implications for offshore site investigations are provided.

Keywords: cone penetrometer test (CPT), cyclic CPT, in-situ testing, offshore.

1. Introduction

The cone penetrometer test (CPT) remains the 'go-to' site investigation tool for offshore in situ investigations. The test protocol (as outlined in ISO 22476-1:2022) involves penetration into the seabed at a constant 2 cm/s with optional pauses at depths of interest for measurement of excess pore pressure dissipation. Although this test protocol has not changed essentially since the electric cone was first used offshore in the early 1970s (Lunne, 2012), recent studies have reported results from CPTs that included cyclic episodes to measure changes in tip resistance and sleeve friction during cycling. These studies were initially in chalk (Diambra et al. 2014) but have since been extended to over consolidated clays (Shonberg et al. 2019) and sands and silts (Brandish-Lowe et al. 2023).

Field evidence (shown in Fig. 1) indicates that cycling the cone reduces sleeve resistance. These cyclic-induced resistance changes may be relevant to pile installation using vibro-drivers (Tsetas et al. 2023) or to pressure-cycled suction bucket installations (Hamdan et al. 2023). In an attempt to provide further insight into the mechanisms that lead to these resistance changes, this paper presents and discusses data from model scale cyclic cone penetrometer tests in kaolin clay and silica sand.

2. Experiments

2.1. Soil samples

The model scale penetrometer tests were conducted in a geotechnical centrifuge in both normally consolidated kaolin clay and dense silica sand. The clay

sample was prepared as a slurry and consolidated in-flight in the centrifuge at an acceleration of 80g over a period of 5 days, with periodic penetrometer testing indicating that this was sufficient for the soil strength to stabilise (and hence for consolidation to complete). The sand sample was prepared in a dry state by air pluviation to achieve a relative density of $D_r = 90\%$, before saturating from the base of the sample with a cellulose ether solution, prepared to achieve a viscosity of 100 cSt (100 times that of water), balancing the centrifuge environment at 100g such that the seepage characteristics were scaled correctly (Bienen et al. 2018). The saturated sand sample was spun to the testing acceleration of 100g and back 3 times before the penetrometer tests in an attempt to 'shake-down' the sample to an equilibrium density state.

2.2. Model scale penetrometers

The tests in clay utilised a model scale piezocone penetrometer with a 60° cone tip and a cone (and shaft) diameter, $D = 10$ mm (see Fig. 2a), and a model scale T-bar penetrometer with a bar diameter, $D = 5$ mm and length, $L = 20$ mm (see Fig. 2b). The T-bar penetrometer has a tip load cell just above the bar, whereas the piezocone has separate load cells to measure tip and sleeve resistance. Pore pressure is measured on the piezocone at the u_2 position using a pressure sensor located in the centre of the cone shaft immediately above the cone tip, with fluid channels connecting the filter position to the sensing diaphragm of the pressure sensor. The filter is a ring of polyethylene, 1.4 mm high and 1 mm deep, with an average pore size of 35 μm . Surface roughness measurements of the 37.5 mm long friction

sleeve (made using a stylus profilometer) gave an average roughness in the range $R_a = 0.5$ to $0.7 \mu\text{m}$.

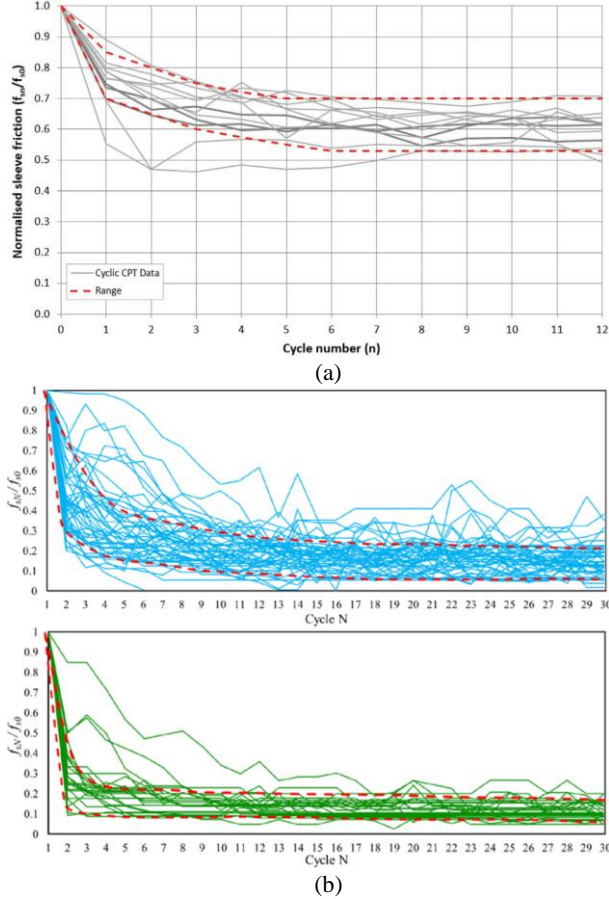


Figure 1. Cyclic CPT data from tests in: (a) North Sea overconsolidated clay (Shonberg et al. 2019) and (b) sand and silt (Brandish-Lowe et al. 2023).

Monotonic cone penetrometer tests in sand utilised the same type of piezocone as for the clay tests but with a higher measurement range for the tip load cell to accommodate the higher penetration resistance in sand. The cyclic cone penetrometer tests in sand used a penetrometer with a diameter, $D = 5 \text{ mm}$. These tests included measurement of both cone tip resistance and total resistance, achieved by locating a load cell at the end of the cone penetrometer shaft. This approach was adopted to provide a basis for interpreting pressure-cycled suction bucket tests that were installed using either suction pressure cycles or ‘jacked’ cycles (Mani et al. 2024a).

2.3. Test procedures

The penetrometers were located on the vertical axis of an electromechanical linear actuator, which was operated in displacement control to penetrate the penetrometers into the samples. Each piezocone test commenced with vertical displacement cycles in the free water above the sample to check that there was no hysteresis in the hydrostatic response of the pressure sensor. The T-bar tests also commenced in the free water above the sample but did not require a cyclic phase in the free water as the T-bar is not instrumented with a pressure sensor. The penetrometers were penetrated in the sample at a velocity, $v = 1 \text{ mm/s}$ to a depth, $z \approx 145 \text{ mm}$ in the clay sample and to $z \approx 80 \text{ mm}$ in the sand sample before

being extracted at the same velocity. The free water cyclic phase above the sample was then repeated for the piezocone tests to check for pore pressure offsets and hysteresis.

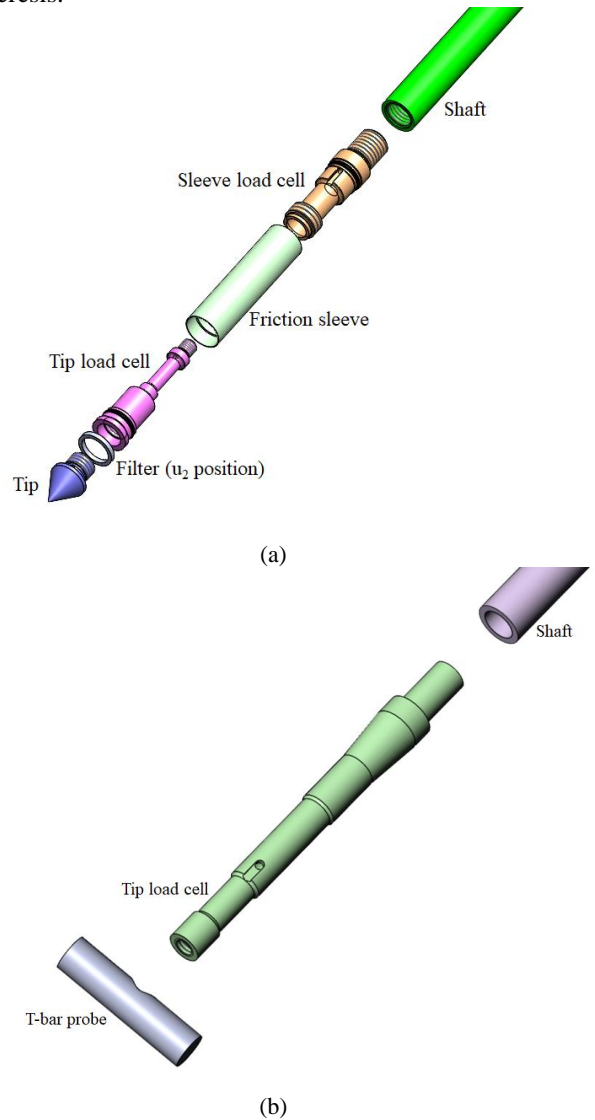


Figure 2. Details of the model scale penetrometers: (a) piezocone and (b) T-bar.

Adopting $c_v = 7 \text{ m}^2/\text{year}$ and $24,200 \text{ m}^2/\text{year}$ for the clay and sand respectively (appropriate for the average initial vertical effective stress in each sample), leads to a dimensionless velocity, $V = vD/c_v = 12$ in the clay and 0.0065 in the sand, such that the response may be considered undrained in the clay and drained in the sand (House et al. 2001; Randolph and Hope 2004; Colreavy et al. 2016).

The cyclic displacement sequence is shown in Fig. 3 and involved vertical displacement by $\pm 2.5 \text{ mm}$ (i.e., $\pm 0.25D$) for the piezocone and $\pm 20 \text{ mm}$ (i.e., $\pm 4D$) for the T-bar over $N = 20$ cycles at a depth, $z = 130 \text{ mm}$. Throughout the paper tip resistance (and the associated soil strength) is reported at a depth measured to the cone shoulder and to the equator position on the T-bar, whereas sleeve resistance is reported at a depth equivalent to the mid-height of the sleeve, accounting for partial embedment (see Fig. 4).

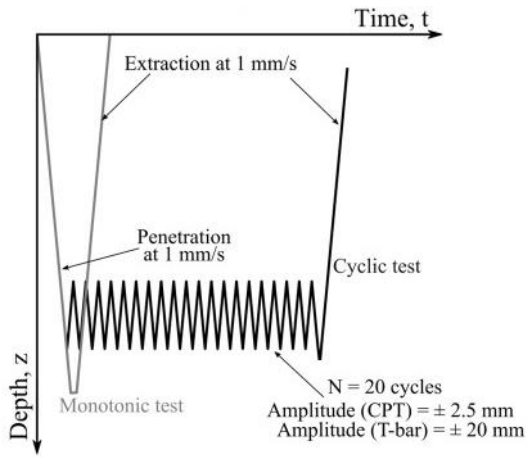


Figure 3. Monotonic and cyclic sequences adopted in the penetrometer tests.

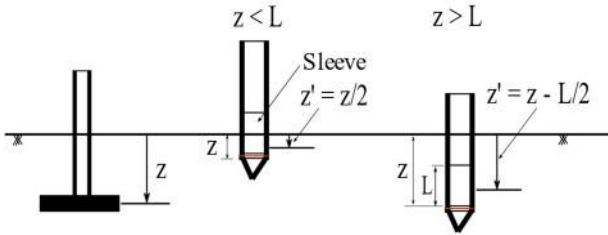


Figure 4. Location on each penetrometer for depth measurement.

3. Results and discussion

3.1. Clay

Depth profiles of undrained shear strength, s_u , in the clay sample are provided in Fig. 5. These profiles were established from the measured T-bar resistance using a T-bar factor, $N_{T\text{-bar}} = 10.5$ (Martin and Randolph 2006), and from the net cone resistance using a cone factor, $N_{kt} = 18$, selected to provide the best overall agreement with the T-bar s_u . Depth (in Fig. 5 and throughout the remainder of the paper) is provided as both an absolute value and normalised by the cone diameter.

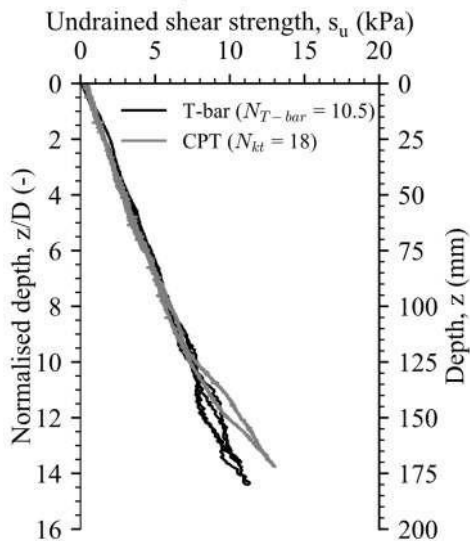


Figure 5. Depth profiles of undrained shear strength in the clay sample.

Fig. 6 compares friction sleeve measurements with both the ‘intact’ undrained shear strength, $s_{u,i}$ (from the piezocone and T-bar) and the strain-softened undrained shear strength during the cyclic phase of the T-bar test. Cycling the T-bar reduces the undrained shear strength to a steady state remoulded value, $s_{u,r}$ that is in reasonable agreement with the sleeve resistance, f_s , indicating that the cone sleeve mobilised the remoulded undrained shear strength. This is consistent with the approach of adopting the remoulded shear strength to quantify frictional resistance of driven piles and suction caissons during installation (e.g., Randolph 2003; Andersen et al. 2005).

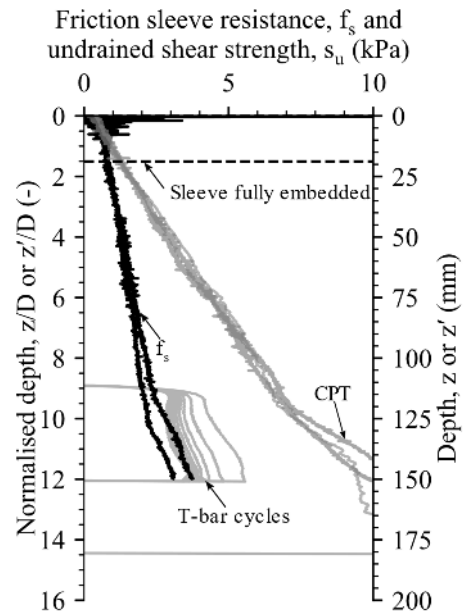


Figure 6. Sleeve friction and undrained shear strength measurements in the clay sample.

Fig. 7 shows changes in frictional sleeve resistance, f_s , as the piezocone was cycled in the clay. In the initial cycles f_s increase to a peak value after about 0.5 mm of movement before reducing to a residual value. This response is attributed to the direction change during shearing at the interface, as observed in cyclic axial friction mobilisation of pipelines (e.g., White et al. 2011). Evidently f_s reduces during the cycles to a value that is lower than the remoulded strength (as the monotonic value of f_s is approximately equal to $s_{u,r}$; see Fig. 6). This degradation is made clear by Fig. 8, which plots normalised values of s_u and f_s against cycle number, N , during cycling of the T-bar and the piezocone. The strength data on Fig. 8 are normalised by the T-bar strength in the initial cycle, $s_{u,0.25}$, where the initial cycle is $N = 0.25$, following the cyclic numbering notation outlined in Randolph et al. (2007).

Cycling the T-bar reduced s_u to 0.38 times the initial value, implying a soil sensitivity, $S_t = 2.6$ (based on penetration resistance), which is typical for this kaolin (e.g., Wang et al. 2023). As shown by Fig. 6, during the initial penetration of the piezocone f_s is approximately equal to the remoulded shear strength, $s_{u,r}$. This is also indicated by Fig. 8, as $f_s/s_{u,0.25}$ at $N = 0.25$ is approximately equal to the stabilised $s_u/s_{u,0.25}$ after $N = 20$ cycles. Cycling the piezocone approximately halved f_s to $f_s/s_{u,0.25} = 0.2$ after about four cycles. Additional cycles

resulted in a subsequent increase in f_s , reaching $f_s/s_{u,0.25} = 0.3$ after the 20 cycles, 25% lower than that mobilised during the initial penetration of the piezocone. This hardening behaviour is considered to be due to dissipation of excess pore pressure induced by the cycles, as also observed by Muhammed et al. (2019) during their small displacement amplitude cyclic tests on a ‘piezoprobe’ in kaolin clay. As discussed in Mani et al. (2024b), the initial reduction in f_s is considered to be due to shear band contraction due to dissipation of excess pore pressure around the sleeve, which reduces the normal stress acting on the sleeve, whereas the subsequent increase is considered to be due to consolidation-induced strength increases.

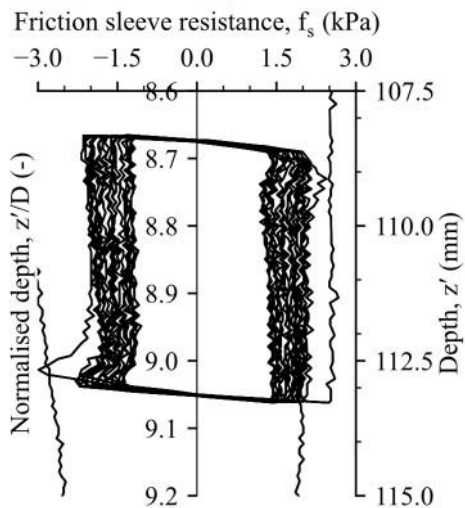


Figure 7. Sleeve friction during cycling in clay.

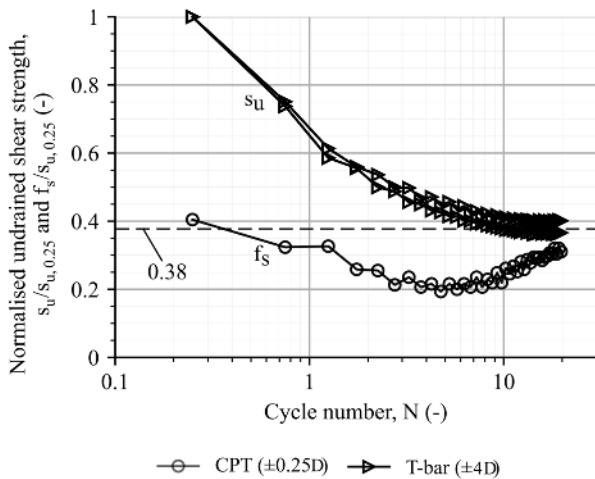


Figure 8. Variation in s_u and f_s during T-bar and cone cycles.

3.2. Sand

Fig. 9 shows depth profiles of shaft friction, f_s , measured in both monotonic and cyclic cone penetrometer tests in the sand. As noted earlier in the paper, these tests utilised a 5 mm diameter cone with measurement of cone tip resistance and total penetration resistance. Shaft friction, f_s , was deduced by subtracting the tip resistance from the total resistance, such that f_s on Fig. 9 represents the average shaft resistance over the embedded shaft length. Fig. 9 shows reasonable agreement between the shaft friction, f_s , measured in the

monotonic and cyclic tests up to the depth at which the cone was cycled. Cycling the cone causes f_s to reduce significantly, particularly in the initial two cycles. The cyclic response is more evident in the inset plot on Fig. 9, which shows mobilisation of peak f_s values within about 0.2 mm during the extraction phase of each cycle, but not when the direction changes. However, localised increases in f_s are also apparent towards the end of each re-penetration, which may be associated with sand infill beneath the cone tip as the cone is moved upwards.

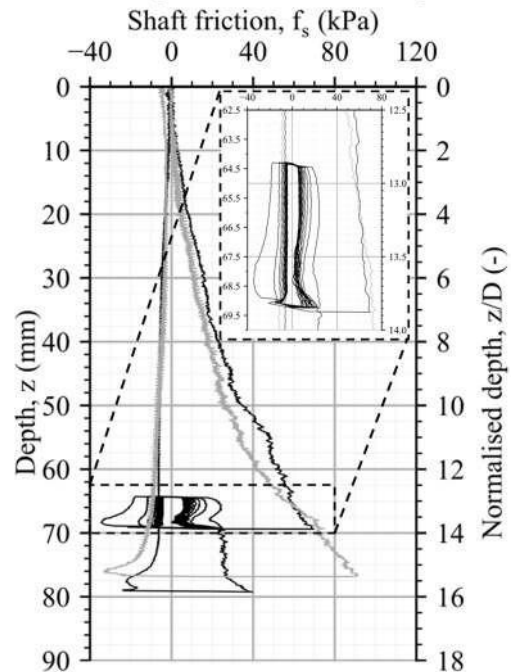


Figure 9. Monotonic and cyclic shaft friction in sand.

The change in f_s during cycling is shown more clearly by Fig. 10, which plots normalised shaft friction, $f_s/f_{s,0.25}$, at the mid height of the cycle against cycle number, N , using the same cyclic numbering notation adopted for the tests in clay (see Fig. 8). Unlike the tests in clay, f_s is lower in extraction than in penetration due to the reduction in normal stress on the shaft during extraction. Shaft friction after the 20 cycles reduces to just less than 20% of the monotonic value during penetration and about 5% of the monotonic value during extraction.

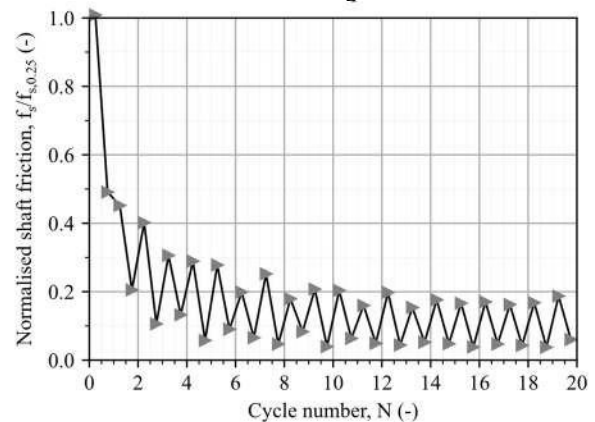


Figure 10. Variation in shaft friction during cycling in sand.

The reduction in f_s shown on Fig. 10 is consistent with the shear band contraction mechanism associated with friction fatigue of piles in sand (white and Lehane, 2004), albeit that the shear band contraction in sand is due to

densification rather than excess pore pressure dissipation. This difference also explains why a hardening response is not observed for the tests in sand, recalling that a drained response is expected for the CPTs in sand.

4. Concluding comments: implications for site investigation

The model scale tests considered in this paper produced cyclic-induced changes in sleeve friction that are broadly consistent with the field measurements shown in Fig. 1. These measurements may be made without modification to the drive and data acquisition systems on current site investigation rigs and may form a useful input to offshore geotechnical designs. However, consideration needs to be given to the implications of modifying test protocols, particularly in view of the very high day rates associated with site investigation vessels.

Assuming a cyclic amplitude of 200 mm, as in the field tests reported in Shonberg et al. (2019), and the standard 2 cm/s penetrometer velocity, then the duration for 20 cycles would be just over 6.5 minutes. To put this in context, this duration is equivalent to increasing the penetration depth of the cone by 4 m, and is insignificant relative to typical durations associated with the dissipation phase of a cone penetration test in fine-grained soils. For example, the Teh and Houlsby (1991) solution indicates that 80 minutes would be required for the T_{50} duration (i.e., 50% dissipation), assuming a 10 cm² cone in a soil with a rigidity index, $I_r = 100$ and a coefficient of consolidation, $c_h = 5$ m²/year.

The tests reported here did not include a dissipation phase before the cyclic movements, such that for the tests in clay, excess pore pressure generated during the initial penetration would be dissipating during the cycles. This has the potential to complicate interpretation of the measured sleeve friction during cycling. Avoiding this would require a dissipation period before conducting the cycles, probably at least to T_{75} , but potentially to T_{90} . For the soil with $c_h = 5$ m²/year considered above, the T_{75} dissipation period would be approximately 6 hours, which is unlikely to be economically viable for the majority of offshore site investigations. This predicament is likely to be avoided in coarser-grained soils as the initial penetration would be either drained, or dissipation would be rapid. For instance, the T_{75} dissipation period reduces to approximately 18 minutes for a soil with $c_h = 100$ m²/year (i.e., a representative value for a sandy silt).

In summary, the value of including a cyclic phase in a CPT is clear for coarser-grained soils as the new test protocol has little implication for operations or cost. The value proposition in fine-grained soils is less clear and will depend on whether changes in sleeve friction measured without a preceding dissipation phase can be interpreted to provide data that are useful in design.

Acknowledgements

This work forms part of the activities of the Centre for Offshore Foundation Systems (COFS) and the Fugro Chair in Geotechnics. This study is part of an Australian

Research Council Linkage Project (Project grant No.: LP180100024).

References

- Andersen, K.H., Murff, J.D., Randolph, M.F., Clukey, E.C., Erbrich, C.T., Jostad, H.P., Hansen, B., Aubeny, C., Sharma, P. and Supachawarote, C. (2005). Suction anchors for deepwater applications. Proceedings of the 1st International Symposium on Frontiers in Offshore Geotechnics, ISFOG, 3-30.
- Bienen, B., Klinkvort, R.T., O'Loughlin, C.D., Zhu, F. and Byrne, B. (2018). Suction caissons in dense sand, part I: Installation, limiting capacity and drainage, *Géotechnique*, 68(11), 937-952, <https://doi.org/10.1680/jgeot.16.P.281>
- Brandish-Lowe, C.S., Masters, T.A., Shonberg, A. and Harte, M. (2023). Comparative assessment of differing in-situ degradation behaviour in offshore silt and sand soils using cyclic and dual sleeve piezocone penetration tests, Proceedings of the 9th International Offshore Site Investigation and Geotechnics Conference, Innovative Geotechnologies for Energy Transition, Vol. 1, 352-359.
- Colreavy, C., O'Loughlin, C.D. and Randolph, M.F. (2016). Experience with a dual pore pressure element piezoball, *International Journal of Physical Modelling in Geotechnics*, 16(3), 101-118, <https://doi.org/10.1680/jphmg.15.00011>
- Diambra, A., Ciavaglia, F., Harman, A., Dimelow, C., Carey, J. and Nash, D.F.T. (2014). Performance of cyclic cone penetration tests in chalk. *Géotechnique Letters*, 4(3), 230-237, <https://doi.org/10.1680/geolett.14.00050>
- Hamdan, N., Powell, T.A., MacBeath, M., Joseph, T., Mallikarachchi, H. and Jones, L. (2023). Cyclic installation of suction caissons: and overview of mitigating the effect of pressure cycling on the tensile resistance – Part IV, Proceedings of the 9th International Offshore Site Investigation and Geotechnics Conference, Innovative Geotechnologies for Energy Transition, Vol. 3, 1741-1748.
- House, A.R., Oliveira, J.R.M.S. and Randolph, M.F. (2001). Evaluating the coefficient of consolidation using penetration tests. *International Journal of Physical Modelling in Geotechnics*, 1, 17-26, <https://doi.org/10.1680/ijpmg.2001.010302>
- Lunne, T. (2012). The fourth James K. Mitchell Lecture: The CPT in offshore soil investigations – a historical perspective, *Geomechanics and Geoengineering*, 7(2), 75-101, <https://doi.org/10.1080/17486025.2011.640712>
- Mani, S., Bienen, B. and O'Loughlin, C.D. (2024a). Pressure cycled installation of suction buckets in sand and layered soil profiles, *ASCE Journal of Geotechnical and Geoenvironmental Engineering*, under review.
- Mani, S., O'Loughlin, C.D., Bienen, B. and Bransby, F. (2024b). Experimental observations from cyclic cone penetrometer testing in clay, *Géotechnique*, under review.
- Martin, C.M. and Randolph, M.F. (2006). Upper-bound analysis of lateral pile capacity in cohesive soil. *Géotechnique*, 56(2), 141-145, <https://doi.org/10.1680/geot.2006.56.2.141>
- Muhammed, R.D., Canou, J., Dupla, J.-C. and Tabbagh, A. (2019). Evaluation of local friction and pore-water pressure evolution along instrumented probes in saturated clay for large numbers of cycles. *Canadian Geotechnical Journal*, 56, 1953-1967, <https://doi.org/10.1139/cgj-2017-0408>
- Randolph, M.F., Low, H.E., and Hongjie Z. (2007). In situ testing for design of pipeline and anchoring systems. Proceedings of the International Offshore Site Investigation and Geotechnics Conference, Confronting New Challenges and Sharing Knowledge, paper no. SUT-OSIG-07-251.
- Randolph, M.F. (2003). Science and empiricism in pile foundation design. *Géotechnique*, 53(10), 847-875, <https://doi.org/10.1680/geot.2003.53.10.847>
- Randolph, M.F. and Hope, S. (2004). Effect of cone velocity on cone resistance and excess pore pressures.

Proceedings of the International Symposium on Engineering Practice and Performance of Soft Deposits, 147–152.

Shonberg, A., Harte, M., Tucker, G., Rattley, M. and Gibbs, P. (2019). Innovative Use of the CPT to assess the in situ degradation of an offshore overconsolidated clay, Proceedings of the Offshore Technology Conference, paper no. OTC-29414, <https://doi.org/10.4043/29414-MS>

Teh, C.I. and Houlsby, G.T. (1991). An analytical study of the cone penetration test in clay, *Géotechnique*, 41(1), 17-34, <https://doi.org/10.1680/geot.1991.41.1.17>

Tsetas, A., Tsouvalas, A., Gómez, S.S., Pisanò, F., Kementzetzidis, E., Molenkamp, T., Elkadi, A.S.K. and Metrikine, A.V. (2023). Gentle Driving of Piles (GDP) at a sandy site combining axial and torsional vibrations: Part I - installation tests, *Ocean Engineering*, 270, 113453, <https://doi.org/10.1016/j.oceaneng.2022.113453>

Wang, C., O'Loughlin, C.D., Bransby, F., Watson, P. and Zhou, Z. (2023). Consolidation-induced improvements in plate anchor capacity, *Canadian Geotechnical Journal*, 60(8), 1264-1275, <https://doi.org/10.1139/cgj-2022-0382>

White D.J., Bruton, D.A.S., Bolton, M., Hill, A.J., Ballard, J-C. and Langford, T. (2011). SAFEBUCK JIP – Observations of axial pipe-soil interaction from testing on soft natural clays. Proceedings of the Offshore Technology Conference, paper no. OTC-29414, <https://doi.org/10.4043/21249-MS>

White, D.J. and Lehane, B.M. (2004). Friction fatigue on displacement piles in sand. *Géotechnique*, 54(10), 645-658, <https://doi.org/10.1680/geot.2004.54.10.645>